Fast prototyping using 3D printed templates and flexible fluoropolymer microcapillary films offers enhanced micromixing in immobilised (bio)catalytic reactions

Kirandeep K. Gill[a], Zhengchun Liu[b] and Nuno M. Reis[a]

[a]*Department of Chemical Engineering and Centre for Biosensors, Bioelectronics and Biodevices (C3Bio), University of Bath, Bath BA2 7AY, United Kingdom*

[b]*Hunan Key Laboratory for Super Microstructure and Ultrafast Process, Department of Electronic Information Science and Technology, School of Physics and Electronics, Central South University, Changsha, Hunan 410083, People's Republic of China*

Abstract

Microreactors offer large surface-area-to-volume (SAV) ratios and short diffusion distances, yet, even at sub-millimetre space, there remains a level of mass transfer control of reactions. This can be minimised using passive micromixers currently requiring access to advanced microfabrication techniques. We report the fast fabrication and in-depth micromixing characterisation of inexpensive non-linear microstructure prototypes using, for the first time, a flexible fluoropolymer microcapillary film (MCF) re-shaped, post-extrusion, with 3D printed templates offering in-flow enhancement of mass transfer in immobilised (bio)catalytic reactions not previously studied for this type of micro-engineered materials. The versatile "push-and-click" 3D printed templates allow one-step production of multi-bored, non-invasive micromixers with simple architectures, namely 'square', 'zigzag' and 'wavy' geometries without the short length restrictions of conventional microfluidic devices. The passive micromixers were numerically evaluated using Computational Fluid Dynamics (CFDs) and extensively validated experimentally using novel residence time distribution (RTD) data which assessed the role of Reynold numbers (0.6 – 60) and molecular diffusion coefficients (10^{-6} – 10^{-11} m^2/s), providing significant in-depth understanding of fluid flow distribution. By evaluating the in-flow oxidative coupling reaction of o-phenylenediamine (OPD, a chromogenic substrate) to 2,3-diaminophenazine (DAP) with an immobilised enzyme, horseradish peroxidase (HRP), we demonstrated the reaction rates in the 'square' and 'zigzag' (sharp bends) were improved by ~43 and ~46% respectively, compared to straight microcapillaries. This is linked to enhanced radial fluid movement. The proposed prototypes can be readily tailored for facilitated fabrication of practical high-performance microreactors suited for heterogeneous assays or in-flow (bio)catalytic reactions in non-microdevice dedicated labs.

Keywords: Micromixers, microreactor, RTD, immobilised enzymatic reactions, 3D printing, mass transfer

1. Introduction

Miniaturized systems offer fast micromixing through reduced diffusion times given that the distance molecules need to travel in microchannels decreases in proportion to the square of the channel diameter [1]. However, reaction rates are still limited as diffusive mixing across fluidic interfaces is inherently slow and inefficient [2]. As turbulent mixing cannot be realized at the microscale, much effort has gone into the design of microfluidic devices for rapidly mixing fluids [3], [4]. Nevertheless, such devices often have high costs and require invasive and complex manufacturing methods [5], [6], including a clean lab for microfabrication. Therefore, there is a need for high performance micromixers produced through rapid and inexpensive fabrication methods suitable for practical applications and easy adaptation.

Micromixing devices can be classed as passive or active [7]. Passive devices depend on geometric properties of the channel or intrinsic hydrodynamic forces, whereas active devices use time dependent external factors, such as acoustic forces [8], thermal actuation [9] or magnetohydrodynamic flow [10]. Additionally, chaotic micromixers with twisted microchannels [11], modified geometries [12], and microchannels with internal structures such as obstructions [13], staggered herringbone grooves [14], valves [15] and lamination patterns [16] have been investigated as passive devices. The introduction of obstacles within microchannels and narrowing of mixing channels are effective in improving mixing efficiency yet are relatively difficult to fabricate and lead to an increase in pressure drop [17], [18]. In consideration of these techniques, altering the planar structure of microchannels is non-invasive, simple, and robust.

Ideal mixing in microfluidic devices is of the utmost importance in the performance of biological and chemical analyses. Micromixers aim to overcome radial mass transport limitations by increasing the contact interfacial area between reagent molecules and reducing

diffusion path distance [19]. High flow rates are often utilized to improve the performance of micromixers constrained by the diffusive mixing regime [20]. In contrast with reactions within laminar flow which are governed by interdiffusion, complete micromixing fully homogenises species in a mixture at the molecular level and directly impacts product conversion and reaction rates [21].

The field of microfluidics has evolved from first generation planar micro machining photolithography and etching fabrication techniques to the revolution of soft lithography [22] and paper microfluidics [23] and is currently progressing towards three-dimensional (3D) printing [24]. 3D printing is a relatively inexpensive technology that can produce complex 3D structures with a high resolution from digital designs and offers several advantages such as: (1) requiring no clean-room, (2) high versatility and (3) structures can be manufactured in one step [25]. 3D printed devices have been implemented in a broad range of areas such as droplet microfluidics [26] as well as and biological [27] and chemical applications [28]. The main limitation of directly printing microfluidic devices is the lack of suitable resins that possess the desired optical, chemical and biocompatibility properties [29], [30].

Implementing enzymatic assays in microfluidic devices offers advantages such as reduced reagent consumption and portability, though reaction times remain slow as the microchannel systems rely on diffusional mixing [31]. The mass transport process is an important challenge in heterogeneous assays, limiting antigen transport to the receptor surface for reduced sensitivities and long incubation times. Micromixers have been employed to increase the flux of the analyte in assays through the use of acoustic techniques [32], filters [33], nanoparticles [34] and droplets [35]. Reducing the diffusion length is especially important in assays given that substrates often have low molecular diffusivities and require long time periods for complete molecular diffusion [36].

In this study, we used 3D printing to produce a range of 3D templates offering easy, one-step non-invasive re-shaping of micro-engineered, fluoropolymer microcapillary films (MCFs) as a strategy for yielding enhanced radial mixing, exploiting the flexibility, excellent optical properties and straightforward (bio)catalyst immobilisation on the inner wall of the hydrophobic microcapillaries. The melt-extrusion of the MCF material has been extensively published [37], [38], yet this is the first report of immobilized biocatalytic reactions in the MCF using 3D printed templates. Computational Fluid Dynamics (CFD) was used to evaluate numerically the effect of template geometry on micromixing at low Reynolds numbers (*Re*) and experimentally validated with novel residence time distribution (RTD) data representing the degree of axial dispersion in microcapillary flow. We demonstrated the benefit of this new approach in improving the kinetics of conversion of a chromogenic substrate, o-phenylenediamine dihydrochloride (OPD) to 2,3-diaminophenazine (DAP) with horseradish peroxidase (HRP) enzyme passively adsorbed on the inner surface of the microcapillaries, mimicking e.g. (bio)catalytic conversion on the inner wall of the capillaries or a heterogeneous immunoassay.

2. Materials and methods

2.1. Reagents and materials

Rabbit anti-mouse IgG (whole molecule) conjugated with HRP, phosphate buffered solution (PBS), pH 7.4, 10 mM, as buffer and Tween-20 for washings were used in enzymatic assays. The SIGMAFAST OPD tablet set was used for preparation of OPD in urea hydrogen peroxide (H_2O_2) and phosphate-citrate buffer (pH 5). Indigo Carmine dye was used for RTD measurements. All materials were sourced from Sigma-Aldrich (Dorset, UK).

2.2. CFD modelling

ANSYS Fluent Inc. 19.3 was used to numerically simulate 2D fluid flow in different microstructure geometries having internal diameters of 200 µm and domain length 110 mm following a similar method previously reported by Gill et al. [39]. Briefly, using the finite volume method, a planar setup was applied with a pressure-based solver and SIMPLE (Semi-Implicit Method for Pressure-Linked Equations) scheme as the pressure-velocity coupling algorithm. The laminar flow and species transport models were applied. The governing equations for the flow field, assuming isothermal and incompressible Newtonian fluids, were the continuity and Navier-Stokes equations shown in Equations 1 and 2 respectively (ANSYS Inc, 2016):

$$\nabla \cdot \boldsymbol{u} = 0 \tag{1}$$

$$\rho \left[\frac{\partial \boldsymbol{u}}{\partial t} + \boldsymbol{u} \cdot \nabla \boldsymbol{u}\right] = -\nabla p + \eta \nabla^2 \boldsymbol{u} \tag{2}$$

where u is the velocity vector, ρ is density, η is viscosity and t is time. The species concentration distribution was calculated using the convection and diffusion equation shown in Equation 3:

$$\frac{\partial c}{\partial t} + \boldsymbol{u} \cdot \nabla c = D \nabla^2 c \tag{3}$$

where c is the concentration variable and D is diffusion coefficient. Face meshing was used to produce approximately 400,000 quadrilateral elements in a mapped scheme. The element size was adjusted accordingly for microchannel structures with the same number of units (different lengths) to maintain mesh independency.

Water was used as the liquid phase in the CFD simulations with temperature dependant physical properties. The step method approach was used to predict the velocity distribution; here we mimicked a step injection of the tracer by changing the normalized species

concentration from 0 to 1 at the inlet. The area weighted average molar concentration of the species was monitored at the outlet as a function of time. Flow in the microstructures were treated as having open-open boundary conditions, such that there was radial dispersion both upstream and downstream of the reaction section to fairly recreate RTD boundary conditions.

2.3. The flexible, micro-engineered MicroCapillary Film (MCF) material

The 10-bore MCF shown in Figure 1a was fabricated from Teflon FEP by Lamina Dielectrics Ltd. (Billinghurst, West Sussex, UK). The 10-bore, MCF material presented a mean hydraulic diameter, d_h, of 212 ± 16.3 μm; the small degree of variability (6-8%) is intrinsic to the continuous melt-extrusion process used for manufacturing the material [38]. It has been shown previously to an extensive degree that the excellent optical transparency is linked to the refractive index being similar to water and the flat geometry of the film yields a high signal-to-noise (SNR) ratio for optical interrogation/imaging of the strips as the parallel surface of the MCF provides negligible wall refraction effects [38], [41], [42]. The small inner diameter is sufficiently small to experience the effects of molecular diffusion without the impractical pressure drops and reduced volumes of very narrow microcapillaries.

2.4. Design and fabrication of 3D printed templates

Microstructure templates were 3D printed on an ORD Rova 3D printer (ORD Solutions Inc, Canada) which used fused deposition modelling additive manufacturing technology. The microstructures were modelled in 3D with the Autodesk FUSION 360 Software, transformed into G-code using Slic3r and interfaced with the 3D printer using the Pronterface software. The printer bed was set to 110°C and the nozzle temperature to 235°C. The templates were fabricated from acrylonitrile butadiene styrene plastic in approximately 1-3 hours.

2.5. Preparing hydrophilic MCF strips

In this study, flow in the MCF strips relied solely on gravity, siphon effect which required making the microcapillaries hydrophilic. Hydrophilic strips were prepared by incubating 0.1 mg/mL of PVOH solution in the MCF for 2 hours at room temperature. This was followed by washings with 0.05% w/w Tween-20 in PBS using 25 mL syringes and drying by aspirating air.

2.6. Measurement of RTD

The RTD is an important index for understanding the fluid flow in different microreactor configurations. The RTD is an established technique for characterizing and analyzing fluid flow and micromixing, providing a direct measurement of the spread of the residence time of different fluid elements in a given space reactor system. Thus, it provides relevant information regarding dispersion regimes relative to laminar flow and plug flow (no axial dispersion), which directly impacts reaction rates in case of a system with combined dispersion and reaction. A narrow RTD enhances radial micromixing, translating into improved reaction rates, selectively and product yields [43], [44]. A perfect step-in/washout step consisting of dyed tracer breakthroughs were used to measure the RTD in the different microchannel structures with the same length (internal hydraulic volume of 0.1 mL) and same number of units. The MCF strips were initially primed with DI water, after which they were introduced into the inlet well with 200 µL indigo carmine tracer dye (0.5 mg/ml) dissolved in DI water. The concentration of the tracer was measured at the outlet of the strip as a function of time by converting greyscale images from a XS USB 2.0 µEye XS camera (IDS Imaging (Obersulm, Germany) into absorbance values. A white LED backlight (IO Rodeo Inc, US) was used for back illumination (see Figure S1 in supplementary material for detailed setup). The washout

step was generated by switching the inlet feed to a well of 200 µL DI water. The flow rates of the microstructures were kept constant by varying the hydraulic height.

2.7. Analytical modelling of RTD

The cumulative age distribution curve F(t) is defined by the ratio between the outlet concentration (c_{out}) and maximum outlet concentration ($c_{out,max}$) (Equation 1):

$$F(t) = c_{out\ (t)}/c_{out,max} \quad (1)$$

The exit age distribution, E(t), over time (t) is shown in Equation 2 [45]:

$$E(t) = dF(t)/dt \quad (2)$$

The E(Θ) curve (instantaneous normalized concentration) and F(Θ) curve (cumulative) provide normalized concentration profiles which allow us to interpret the dispersion type in the micromixers and compare different mixers using θ, where is $\theta = t/\bar{t}$, which accounts for the time scale or hydraulic times for different systems. The concentration distribution along the length of the capillary in the (i) CFD simulations was measured using the area weighted average of the molar concentration at the outlet over time and in the (ii) experimental RTD we studied the path distance average. Laminar flow in the microfluidic capillaries had the predictable parabolic Gaussian concentration profile in the absence of molecular diffusion or axial dispersion.

2.8. Quantification of chromogenic substrate reaction rates

Conversion of OPD in the microreactors with HRP immobilised on the inner walls were assessed by studying the oxidative coupling of the well-known chromogenic substrate OPD to

DAP product. Our research group has previously shown that the molar ratio of OPD:H_2O_2 is significant and that a value of 1:3, as recommended by suppliers, inhibits the catalytic activity of the HRP enzyme [46]. Our enzymatic studies therefore used the ideal molar ratio of 1:1 for OPD:H_2O_2, equivalent to OPD (MW = 108.1 g/mol) and H_2O_2 (MW = 34.0 g/mol) concentrations of 4 mg/ml and 1 mg/ml respectively, for a higher colorimetric signal [46]. Stock solutions were prepared using the SIGMAFAST OPD tablet set by dissolving OPD solutions (8 mg tablet) in urea- H_2O_2 and phosphate-citrate buffer (8 mg tablet) as required. Diluted solutions were prepared with DI water and the solutions were kept in the dark at room temperature and used within 3 hr. The enzymatic rates of OPD conversion were determined using a range of OPD and HRP concentrations. We passively adsorbed anti-IgG antibodies conjugated to peroxidase, diluted accordingly from a stock solution of 10.6 mg/ml, on the inner surface of the MCF capillaries, incubated for 1.5 hours at room temperature and then incubated PVOH for hydrophilicity following the protocol from Section 2.5. The non-linear microreactors were then fabricated by moulding the strips into the desired shape using the 3D printed templates.

Substrate conversion was examined in continuous microflow reactions which examined reaction rates over the microreactor length. The continuous reaction started by priming the strips with DI water and then flowing 200 µL OPD from the inlet well through 320 mm long MCF strips using siphon action. In our setup flow rate was fully set by gravity, which we measured as 0.93 µl/s. DAP concentration was optically monitored along the reactor length using the camera, as well as over time when the flow stopped (MCF removed from inlet solution). We noticed full conversion within 10-15 minutes, from where the theoretical DAP concentration from the maximum absorbance could be determined.

2.9. Image analysis of microfluidic strips

Digital RGB images of the RTD experiments and enzymatic reactions were split into red, green and blue channels with the ImageJ software (NIH, USA). Using the green channel for maximum SNR, absorbance values were calculated based on the grey scale peak height and averaged across 10 capillaries (Equation 3), as previously reported in our group for colorimetric immunoassays [41], [47]:

$$Abs = -log_{10}\left(\frac{I}{I_0}\right) \quad (3)$$

where I is the grey scale peak height and I_0 is the background grey scale value.

3. Results and discussion

3.1. One-step non-invasive fabrication of non-linear microstructures

Non-linear microstructures were fabricated with 3D printed templates constructed using two blocks of complimentary geometries dependent on the desired final shape of the microreactor (Figure 1b). The adaptability of the fabrication method was apparent through easy modification of designs to produce templates with different aspect ratios and dimensions. Fabrication of the non-linear microstructures involved inserting the MCF in between two 3D printed blocks and applying pressure to bend and reshape the material (Figure 1c). The inherent flexibility of the fluoropolymer material was ideal for conforming to and keeping close to the shape of the template. The one step process offered simplicity without compromising the inner surface of the microchannel.

We highlighted the versatility and easy optimization of template modelling by prototyping three different microstructures, aiming to manipulate fluid flow in ‘wavy’, ‘square’ and ‘zigzag’ geometries whose configurations had gradual to sharp bends with a wide range of bend angles of 180°, 90° and 45° respectively (Figure 2a-c) Due to the nature of post-extrusion re-

shaping these bend angles are approximated and differences quantitatively reported in micromixing/axial dispersion in the sharp and zigzag, fabricated from the same MCF material, are solely related to the geometry. We noted that though the square and zigzag maintain their shape well, the wavy restructures on release from the template and may require external reinforcements (Figure 2d). The MCF material has been previously modified using laser cutting for prototyping of a serpentine micromixer, yet will be impractical and labour intensive for mass production [48]. The 3D printed templates could be manufactured within a few hoursand non-linear microreactors could be re-shaped post-extrusionwithin a few minutes giving a fast production rate.

The importance of manufacturability with minimized total costs and minimal expertise requirements is growing in speciality fields, included decentralized diagnostics. Our 3D printed templates can produce a large number of replicas rapidly and at low cost, using the inexpensive MCF material, and their design with the Computer Aided Design (CAD) models offers the ability to create templates over a wide range of dimensions and with quick iterations between different designs [49], without access to a clean room. Comparatively, conventional methods such as PDMS casting-based 3D moulding (soft lithography) are time consuming and involve manual operations which compromise the accuracy [50]. Additionally, instead of directly 3D printing microstructures which will incur resin costs, our templates can be re-used for a number of times.

3.2.Effect of sharp bends on radial dispersion

We ran simulations for single phase flow in ~200 μm diameter linear microchannels and non-linear geometries whose dimensions matched closely the design of the templates (Figure 3a). There was a strong link between sharp bends (zigzag and square) and an enhanced rate of

transverse exchange between fast- and slow-moving regions, due to pressure and velocity gradient imbalances, for greater radial dispersion. To capture this effect, the mesh grid was refined in the transverse direction of the microchannel, further reducing the element size closer to the laminar boundary layer at the wall (Figure 3b). A mesh independency study determined the optimal grid resolution using the maximum velocity in the microchannels for optimization between numerical accuracy and computational time (Figure 3c). We noticed from velocity contour plots that fluid flow did not significantly deviate from a symmetric Gaussian, parabolic flow velocity profile in the wavy which had gradual turns, whereas sharp bends in the square and zigzag caused flow displacement towards the concave channel wall (Figure 3d). The maximum velocity of the zigzag was 0.12 m/s compared to the theoretical (0.075 m/s) and attributed to enhanced axial dispersion as there was less time for molecules to diffuse radially. Comparatively, the performance of the square was superior through increased radial dispersion with marginal 0.5% peak velocity increase. This was further supported by the markedly lower pressure drop of 101 Pa in the square contrasting with 147 Pa in the zigzag (Table 1).

3.3. Fluid flow profiles in microstructures

We characterized the hydrodynamic behaviour of linear and non-linear microstructures using CFD and experimental breakthrough curves, an important index for assessing fluid flow profiles, at low Reynolds numbers (0.6) and a molecular diffusion coefficient (D_m) of 5×10^{-10} m^2/s matching that of tracer dye [51]. We observe from simulation *E*-curves of the step input that over identical mixing lengths, the square and wavy have a similar RTD to the straight, whilst the zigzag presented the broadest fluid distribution (Figure 4a). The breakthrough curves were directly related to the mean residence times, supported by the small range of $\bar{t}$= 36.9 – 37.4 s for the straight, square, and wavy, indicating minimal velocity increase presumably due to rounder bends, and τ = 21.7 s with the zigzag having sharper bends which translates to greater

axial dispersion）(Table 2). CFD studies were validated with experimental fluid tracing where differences in the zigzag result from a larger bend radius of the microstructure compared to the simulation (Figure 4a). We further observed from CFD breakthrough curves per single unit of microstructure geometry that the square geometry approached closer to near ideal plug flow (Figure 4b(i)). Per single unit, the design of the square microchannel has attractive features for micromixing, exhibiting a longer path length for a relatively high mean hydraulic time and a greater number of fluid flow shifts towards the inner and outer walls (Figure 3e). Therefore, it is expected that the higher number of bends per unit length in the square geometry, and hence increased convective flux of analytes towards receptors on the walls due to frequent fluid flow shifting, will potentially lead to a higher rates of reaction as reagents and products and move more quickly radially compared to mass transport by simple molecular diffusion expected in the straight and wavy geometries. These results were consistent with experimental step in and washout curves (Figure 4b(ii)) for the same number of units(for experimental F-curves see Figure S4 in supplementary material). A large number of studies in literature evaluated the performance of micromixers by the number of units [12], [52], [53], however we have shown using RTD that these studies do not give a true comparison as in these cases path length, rather than geometry, influences the extent of micromixing. Furthermore mixing performance is commonly analysed using a mixing index between two miscible liquids, however our analysis using RTD provides an in depth understanding of the fluid flow profile and can be linked to reaction kinetics via the mean residence time and the extent of axial dispersion [54]. Compared to previous work using the RTD to characterize micromixing in microreactor systems [55], our work enables (i) quantitative and direct comparison between different geometries prepared from exactly the same microengineering material/microcapillary and (ii) a perfect step in/step out using gravity siphon flow implemented experimentally which matches the inlet boundary for the CFD and cannot be replicated by any other technique, including T-mixers, microvalves,

injection valves, to name a few, that result in dead volumes that, although insignificant for microflow systems, greatly compromises the quality of RTD data.

We carried out further CFD investigations on the effects of velocities and diffusion coefficients. The square and straight similarly displayed plug flow at 0.003 m/s (*Re* = 0.6), whilst there was a significant shift towards laminar flow as the velocity increased to 0.05 m/s (*Re* = 10). At the lower velocity, the effect of geometries was less apparent due to molecular diffusion effects (Figure d(i)). This concurred with literature such that there was the diffusion-dominant mixing mechanism at the low velocities and as the velocity increased chaotic advection was enhanced in the micromixer [56], [57]. The optimal velocity was highly dependent on D_m, for example flow was closest to near-ideal plug flow at 0.0003 m/s for $5x10^{-10}$ m^2/s and 0.05 m/s at 10^{-7} m^2/s (Figure 4d). We also noticed for D_m ranging 10^{-6} - 10^{-11} m^2/s that flow was essentially plug flow at higher D_m for all microstructures, with the linear microchannel closest to ideal plug flow, due to the fast diffusion times (see Figure S2 in supplementary material). Consequently, at lower D_m chaotic advection effects were present in non-linear microstructures for higher performance compared to the straight (Figure 4c). Our non-linear microreactors would therefore be suited to (bio)catalytic reactions or heterogeneous reactions/assays, where substrates have low D_m in buffers, and provide increased reaction rates via radial diffusion effects. The 3D templates re-shape microcapillaries post-extrusion for fabrication of non-linear microstructures which enhance radial diffusion effects in a non-invasive manner, without the use of obstacles, for lower pressure drops, reduced shear forces on (bio)catalytic reagents and low chances of clogging with viscous solutions [17], [58]. This is complimented with direct access to the immediate manufacturing of the microreactors requiring minimal expertise.

3.4. Micromixing reactors for heterogeneous enzymatic reactions

We studied the kinetics of substrate conversion in wall immobilised HRP enzyme using the well-known OPD substrate to assess the performance of our surface based microreactors. The HRP/H_2O_2-catalyzed oxidation of OPD (colourless) converts to DAP (orange/brown) and is used frequently in enzyme-linked immunosorbent assays. Here we mimic this by employing a direct one-step assay (Figure 5a), where the fast conversion rate of OPD allows us to kinetically assess the reactions rates, and consequently micromixing, along the length of the microreactors.

Initially we observed the reaction rates over HRP concentrations ranging 5-15 μg/ml with 4 mg/ml OPD at 0.93 μL/s in linear microreactors. Our reactions primed the microreactors with DI water before introducing OPD which allow us to assess micromixing and molecular diffusion effects, whereas an empty microcapillary would focus on interfacial diffusion at the walls. We visually observe that the steady state DAP concentrations were lower than the maximum DAP concentration achieved when flow was stopped (Figure 5b). We expect that the laminar boundary layer from convection limited the radial diffusion at the walls which lowered the DAP yield, consequently when flow stopped the maximum yield increased due to faster diffusion times (Figure 5c). The rate of DAP formation followed Michaelis-Menten kinetics described in Equation 4:

$$-r_s = k_3 C_E \frac{C_S}{C_S + K_m} \tag{4}$$

where k_3 is enzyme turnover number, C_E is enzyme concentration, C_S is substate concentration and K_m is the Michaelis constant. The initial rates of OPD conversion, $-r_s$, along the reactor length was found to be linearly proportional to HRP concentrations (first order) and transitioned into zero order kinetics upon substrate inhibition (Figure 5d). These kinetics were consistent with batch experiments observing OPD conversion (1–4 mg/ml) over time from which we obtained a value of 151.6 ± 11.9 mol_S/min.mol_E (61667 ± 4856 mol_S/min.mol_E) for

k_3 and 1.46 ± 0.05 mg/ml for K_m (see Figure S3 in supplementary material). Our turnover number, k_3, of 1028 $mol_S/s.mol_E$, calculated using $V_{max} = k_3[E]$, from the Michaelis-Menten equation, for enzymes immobilized in the straight capillary in batch experiments was comparable to a similar system assessing the oxidative coupling of OPD to DAP which obtained 1150 1/s using the HRP enzyme in solution [59].

Assessing the reaction rates of the linear microreactors, we used a conjugated HRP concentration of 7 μg/ml to evaluate the performance of our non-linear microreactors as it provided first order kinetics over a longer length. 3D printed templates were fabricated using a template for each geometry, produced in a few hours using rapid additive manufacturing with low-cost materials. Microreactors were imaged from above to give a projected view, however these lengths were transformed into axial lengths (equal microcapillary lengths) for a direct comparison of conversion. Given the low diffusion coefficient of OPD in sodium phosphate buffer, 11.8×10^{-10} m^2/s [60] and at 0.003 m/s (matching RTD studies), we expected the performance of the linear and non-linear microreactors be similar as they approached near plug flow in these conditions (Figure 4a). Yet, we observed $-r_s$ of the square and zigzag were ~43 and ~46% higher than the straight microreactor, respectively, with full conversion achieved over 40 mm which covered a small number of mixing units (2-4) (Figure 5f). Given that the microreactors all had the same path length and same internal diameter (around 200 μm), the major contributing factor to the higher performance of the square and zigzag would then be the convective flux shifts towards the sharp bends due to fluid acceleration which reduced the diffusion distance and increased substrate mass transport to the biocatalyst (enzyme) immobilised on the wall (Figure 5e). Thus, high performance microreactors can be developed at low Reynolds (relevant to bioassays) in a practical and affordable manner. Furthermore, a major benefit of using the 3D printed templates is that the chemical and biocompatibility properties of the structural microengineered material (in this case the MCF) are retained in

contrast to directly printing microfluidic devices for which there is a lack of resins with properties suitable to bioassays [27]. By using MCF, we exploited the excellent optical properties for imaging and simple passive immobilization. Furthermore, fabricating 3D microstructures using our 3D models creates micropatterns using input from CAD software which can increase fabrication complexity with no significant increase time.

Based on our RTD studies, we expected improved reaction rates in the square and zigzag compared to the linear microchannel at higher velocities due to the combined effects of convective flux and greater radial dispersion (Figure 4c). This concurred with current literature showing passive non-linear geometries increase the interfacial area across which diffusion occurs [61], yet we have confirmed this result by gathering experimental RTD data which validated our CFD results. We have demonstrated the importance of convective flux shifts for improved reaction rates and conjecture from RTD studies that, for higher velocities, the relevance of the square and zigzag will be even greater due to the additional effects of increased radial dispersion which will increase analyte capture efficiency at the walls. We noticed enhanced radial dispersion in the zigzag at high Re = 60 due to the smaller bend radius, yet this was outweighed by the 50% ΔP increase compared to the square which may increase shear stresses on biological reagents. A previous study has found that the pressure drop in square-wave and zig-zag channels are approximately the same, yet we believe these results are not truly comparable since they evaluate the number of units rather than the path length [12]. Low mixing efficiency, and hence reaction rates, are expected in the wavy comparative to the straight at low Reynolds numbers due to the gradual curves where velocities sufficient to induce secondary flows will be necessary for improved micromixing. We have tested a single reaction in the microreactors, yet each re-shaped MCF has the capability for multiplexing using the 10 parallel bores in the MCF material.

The 3D printed templates are practical and highly versatile as the number of units and microreactor length can be easily optimized for specific reactions and fabricated within a few minutes. The non-invasive fabrication technique offers the benefit of reducing shear forces on (bio)catalytic reagents which are imposed by the addition of obstacles in micromixers. Furthermore, the Teflon® FEP material of the MCF offers several advantages to carry out a multitude of wall-immobilised bio-catalytic reactions as it provides excellent chemical resilience, simple passive adsorption of proteins/enzymes and can accommodate for temperature dependant reactions. 3D printing technologies are rapidly growing with future techniques having potential advances such as resolution improvements and increased number of thermoplastics with better biocompatible and optical properties and is expected to take a leading technological role in global health care, mostly prototyping diagnostic devices for the third world [30], as supported by our prototypes which can be developed in non-microdevice dedicated laboratories with minimal training.

4. Conclusions

We demonstrated a new and simple approach for the fast one-step fabrication of inexpensive micromixer prototypes using 3D printed templates and flexible mass-manufacturable MCF material. CFD studies validated with novel RTD breakthrough curves significantly relevant for hydrodynamic characterization demonstrated a strong link between sharp bends in the square and zigzag and enhancement of radial dispersion at low D_m. We further showed the reduced relevance of micromixing in non-linear microstructures at high D_m due to the shorter diffusion distances of species between the bulk and the wall having the immobilised enzyme/biocatalyt. This is the first report showing application of the MCF to immobilized biocatalytic reactions fabricated into non-linear microreactors using 3D printed templates. An oxidative coupling reaction with HRP enzyme in our microreactors revealed increased substrate mass transport to

the biocatalyst immobilised on the wall in the square and zigzag, via reduced diffusion distance, leading to increased $-r_s$ by ~43 and ~46% respectively (Re = 0.6) compared to the straight, demonstrating high performance microreactors can be developed at low Reynolds numbers relevant to bioassays. The square was deemed to be superior at low Re as the zigzag had lower mean residence times (21.7 compared to 37.4 s) and a 46% ΔP increase. The bends in geometries are a significant parameter for inducing alternating radial flow shifts of analytes towards immobilized enzymes on the inner and outer walls, where the square has the higher number of bends per unit length, leading the higher capture efficiencies and reaction rates. Furthermore, continuous flow of enzymatic substrate was found to limit the maximum conversion of OPD compared to stopped flow. The proposed microstructure prototypes can be readily tailored to suit specific reactions involve immobilised (bio)catalyst through easy modification of length, geometry, and number of units for practical inexpensive high-performance microreactors suited for surface-based reactions.

Acknowledgements

K.K. Gill is grateful to EPSRC and University of Bath for financial support through funding a Ph.D. scholarship.

References

[1] D. Janasek, J. Franzke, and A. Manz, "Scaling and the design of miniaturized chemical-analysis systems," *Nature*, vol. 442, no. 7101, pp. 374–380, 2006, doi: 10.1038/nature05059.

[2] A. J. DeMello, "Control and detection of chemical reactions in microfluidic systems," *Nature*, vol. 442, no. 7101, pp. 394–402, 2006, doi: 10.1038/nature05062.

[3] C. Y. Lee, C. L. Chang, Y. N. Wang, and L. M. Fu, "Microfluidic mixing: A review," *Int. J. Mol. Sci.*, vol. 12, no. 5, pp. 3263–3287, 2011, doi: 10.3390/ijms12053263.

[4] T. J. Johnson, D. Ross, and L. E. Locascio, "Rapid microfluidic mixing," *Anal. Chem.*, vol. 74, no. 1, pp. 45–51, 2002, doi: 10.1021/ac010895d.

[5] E. A. Mansur, M. YE, Y. WANG, and Y. DAI, "A State-of-the-Art Review of Mixing in Microfluidic Mixers," *Chinese J. Chem. Eng.*, vol. 16, no. 4, pp. 503–516, 2008, doi: 10.1016/S1004-9541(08)60114-7.

[6] H. A. Stone, A. D. Stroock, and A. Ajdari, "Engineering Flows in Small Devices," *Annu. Rev. Fluid Mech.*, vol. 36, no. 1, pp. 381–411, 2004, doi: 10.1146/annurev.fluid.36.050802.122124.

[7] J. Zhang *et al.*, "Fundamentals and applications of inertial microfluidics: A review," *Lab Chip*, vol. 16, no. 1, pp. 10–34, 2016, doi: 10.1039/c5lc01159k.

[8] D. Ahmed, X. Mao, B. K. Juluri, and T. J. Huang, "A fast microfluidic mixer based on acoustically driven sidewall-trapped microbubbles," *Microfluid. Nanofluidics*, vol. 7, no. 5, pp. 727–731, 2009, doi: 10.1007/s10404-009-0444-3.

[9] B. Xu, T. N. Wong, N. T. Nguyen, Z. Che, and J. C. K. Chai, "Thermal mixing of two miscible fluids in a T-shaped microchannel," *Biomicrofluidics*, vol. 4, no. 4, pp. 1–13, 2010, doi: 10.1063/1.3496359.

[10] Y. Wang, J. Zhe, B. T. F. Chung, and P. Dutta, "A rapid magnetic particle driven micromixer," *Microfluid. Nanofluidics*, vol. 4, no. 5, pp. 375–389, 2008, doi: 10.1007/s10404-007-0188-x.

[11] C. P. Jen, C. Y. Wu, Y. C. Lin, and C. Y. Wu, "Design and simulation of the micromixer with chaotic advection in twisted microchannels," *Lab Chip*, vol. 3, no. 2, pp. 77–81, 2003, doi: 10.1039/b211091a.

[12] S. Hossain, M. A. Ansari, and K. Y. Kim, "Evaluation of the mixing performance of three passive micromixers," *Chem. Eng. J.*, vol. 150, no. 2–3, pp. 492–501, 2009, doi: 10.1016/j.cej.2009.02.033.

[13] A. A. S. Bhagat, E. T. K. Peterson, and I. Papautsky, "A passive planar micromixer with obstructions for mixing at low Reynolds numbers," *J. Micromechanics Microengineering*, vol. 17, no. 5, pp. 1017–1024, 2007, doi: 10.1088/0960-1317/17/5/023.

[14] M. S. Williams, K. J. Longmuir, and P. Yager, "A practical guide to the staggered herringbone mixer," *Lab Chip*, vol. 8, no. 7, pp. 1121–1129, 2008, doi: 10.1039/b802562b.

[15] C. C. Hong, J. W. Choi, and C. H. Ahn, "A novel in-plane passive microfluidic mixer with modified Tesla structures," *Lab Chip*, vol. 4, no. 2, pp. 109–113, 2004, doi: 10.1039/b305892a.

[16] T. Tofteberg, M. Skolimowski, E. Andreassen, and O. Geschke, "A novel passive micromixer: Lamination in a planar channel system," *Microfluid. Nanofluidics*, vol. 8, no. 2, pp. 209–215, 2010, doi: 10.1007/s10404-009-0456-z.

[17] A. S. Yang *et al.*, "A high-performance micromixer using three-dimensional Tesla structures for bio-applications," *Chem. Eng. J.*, vol. 263, pp. 444–451, 2015, doi: 10.1016/j.cej.2014.11.034.

[18] Y. Li, D. Zhang, X. Feng, Y. Xu, and B. F. Liu, "A microsecond microfluidic mixer for characterizing fast biochemical reactions," *Talanta*, vol. 88, pp. 175–180, 2012, doi: 10.1016/j.talanta.2011.10.028.

[19] M. Rahimi, N. Azimi, M. A. Parsamogadam, A. Rahimi, and M. M. Masahy, "Mixing performance of T, Y, and oriented Y-micromixers with spatially arranged outlet channel: evaluation with Villermaux/Dushman test reaction," *Microsyst. Technol.*, vol. 23, no. 8, pp. 3117–3130, 2017, doi: 10.1007/s00542-016-3118-6.

[20] V. Mengeaud, J. Josserand, and H. H. Girault, "Mixing processes in a zigzag microchannel: Finite element simulations and optical study," *Anal. Chem.*, vol. 74, no. 16, pp. 4279–4286, 2002, doi: 10.1021/ac025642e.

[21] C. P. Fonte, D. F. Fletcher, P. Guichardon, and J. Aubin, "Simulation of micromixing in a T-mixer under laminar flow conditions," *Chem. Eng. Sci.*, vol. 222, pp. 1–10, 2020, doi: 10.1016/j.ces.2020.115706.

[22] D. C. Duffy, J. C. McDonald, O. J. A. Schueller, and G. M. Whitesides, "Rapid prototyping of microfluidic systems in poly(dimethylsiloxane)," *Anal. Chem.*, vol. 70, no. 23, pp. 4974–4984, 1998, doi: 10.1021/ac980656z.

[23] X. Li, D. R. Ballerini, and W. Shen, "A perspective on paper-based microfluidics: Current status and future trends," *Biomicrofluidics*, vol. 6, no. 1, 2012, doi: 10.1063/1.3687398.

[24] S. Waheed *et al.*, "3D printed microfluidic devices: Enablers and barriers," *Lab Chip*, vol. 16, no. 11, pp. 1993–2013, 2016, doi: 10.1039/c6lc00284f.

[25] H. N. Chan, Y. Chen, Y. Shu, Y. Chen, Q. Tian, and H. Wu, "Direct, one-step molding of 3D-printed structures for convenient fabrication of truly 3D PDMS microfluidic chips," *Microfluid. Nanofluidics*, vol. 19, no. 1, pp. 9–18, 2015, doi: 10.1007/s10404-014-1542-4.

[26] J. M. Zhang, Q. Ji, and H. Duan, "Three-dimensional printed devices in droplet microfluidics," *Micromachines*, vol. 10, no. 11, pp. 1–24, 2019, doi: 10.3390/mi10110754.

[27] C. M. B. Ho, S. H. Ng, K. H. H. Li, and Y. J. Yoon, "3D printed microfluidics for biological applications," *Lab Chip*, vol. 15, no. 18, pp. 3627–3637, 2015, doi: 10.1039/c5lc00685f.

[28] Y. He, Y. Wu, J. Z. Fu, Q. Gao, and J. J. Qiu, "Developments of 3D Printing Microfluidics and Applications in Chemistry and Biology: a Review," *Electroanalysis*, vol. 28, no. 8, pp. 1658–1678, 2016, doi: 10.1002/elan.201600043.

[29] A. I. Shallan, P. Smejkal, M. Corban, R. M. Guijt, and M. C. Breadmore, "Cost-effective three-dimensional printing of visibly transparent microchips within minutes," *Anal. Chem.*, vol. 86, no. 6, pp. 3124–3130, 2014, doi: 10.1021/ac4041857.

[30] N. Bhattacharjee, A. Urrios, S. Kang, and A. Folch, "The upcoming 3D-printing revolution in microfluidics," *Lab Chip*, vol. 16, no. 10, pp. 1720–1742, 2016, doi: 10.1039/c6lc00163g.

[31] A. G. Hadd, D. E. Raymond, J. W. Halliwell, S. C. Jacobson, and J. M. Ramsey, "Microchip Device for Performing Enzyme Assays," *Anal. Chem.*, vol. 69, no. 17, pp. 3407–3412, 1997, doi: 10.1021/ac970192p.

[32] Y. Gao, P. Tran, K. Petkovic-Duran, T. Swallow, and Y. Zhu, "Acoustic micromixing increases antibody-antigen binding in immunoassays," *Biomed. Microdevices*, vol. 17, no. 4, pp. 1–5, 2015, doi: 10.1007/s10544-015-9987-0.

[33] Y. Ukita *et al.*, "Application of vertical microreactor stack with polystylene microbeads to immunoassay," *Sensors Actuators, A Phys.*, vol. 145–146, no. 1–2, pp. 449–455, 2008, doi: 10.1016/j.sna.2008.01.024.

[34] K. Petkovic *et al.*, "Rapid detection of Hendra virus antibodies: an integrated device with nanoparticle assay and chaotic micromixing," *Lab Chip*, vol. 17, no. 1, pp. 169–177, 2017, doi: 10.1039/c6lc01263a.

[35] M. Y. H. Tang and H. C. Shum, "One-step immunoassay of C-reactive protein using droplet microfluidics," *Lab Chip*, vol. 16, no. 22, pp. 4359–4365, 2016, doi: 10.1039/c6lc01121g.

[36] K. Ishii, E. Hihara, and T. Munakata, "Mechanism of temperature-difference-induced spiral flow in microchannel and investigation of mixing performance of a non-invasive micromixer," *Appl. Therm. Eng.*, vol. 174, no. November 2019, p. 115291, 2020, doi: 10.1016/j.applthermaleng.2020.115291.

[37] B. Hallmark, F. Gadala-Maria, and M. R. Mackley, "The melt processing of polymer microcapillary film (MCF)," *J. Nonnewton. Fluid Mech.*, vol. 128, no. 2–3, pp. 83–98, 2005, doi: 10.1016/j.jnnfm.2005.03.013.

[38] A. D. Edwards, N. M. Reis, N. K. H. Slater, and M. R. MacKley, "A simple device for multiplex ELISA made from melt-extruded plastic microcapillary film," *Lab Chip*, vol. 11, no. 24, pp. 4267–4273, 2011, doi: 10.1039/c0lc00357c.

[39] K. K. Gill, R. Gibson, K. H. C. Yiu, P. Hester, and N. M. Reis, “Microcapillary film reactor outperforms single-bore mesocapillary reactors in continuous flow chemical reactions,” *Chem. Eng. J.*, vol. 408, no. September 2020, p. 127860, 2021, doi: 10.1016/j.cej.2020.127860.

[40] ANSYS Inc, “ANSYS Fluent User’s Guide, Release 17.2,” 2019.

[41] A. I. Barbosa, P. Gehlot, K. Sidapra, A. D. Edwards, and N. M. Reis, “Portable smartphone quantitation of prostate specific antigen (PSA) in a fluoropolymer microfluidic device,” *Biosens. Bioelectron.*, vol. 70, pp. 5–14, 2015, doi: 10.1016/j.bios.2015.03.006.

[42] A. P. Castanheira, A. I. Barbosa, A. D. Edwards, and N. M. Reis, “Multiplexed femtomolar quantitation of human cytokines in a fluoropolymer microcapillary film,” *Analyst*, vol. 140, no. 16, pp. 5609–5618, 2015, doi: 10.1039/c5an00238a.

[43] M. H. Reis, T. P. Varner, and F. A. Leibfarth, “The Influence of Residence Time Distribution on Continuous-Flow Polymerization,” *Macromolecules*, vol. 52, no. 9, pp. 3551–3557, 2019, doi: 10.1021/acs.macromol.9b00454.

[44] A. Cantu-Perez, S. Barrass, and A. Gavriilidis, “Hydrodynamics and reaction studies in a layered herringbone channel,” *Chem. Eng. J.*, vol. 167, no. 2–3, pp. 657–665, 2011, doi: 10.1016/j.cej.2010.10.044.

[45] O. Levenspeil, *Chemical Reaction Engineering*. New York: Wiley, 1999.

[46] A. I. Barbosa, A. P. Castanheira, and N. M. Reis, “Sensitive optical detection of clinically relevant biomarkers in affordable microfluidic devices: Overcoming substrate

diffusion limitations," *Sensors Actuators, B Chem.*, 2018, doi: 10.1016/j.snb.2017.11.086.

[47] A. I. Barbosa, A. P. Castanheira, A. D. Edwards, and N. M. Reis, "A lab-in-a-briefcase for rapid prostate specific antigen (PSA) screening from whole blood," *Lab Chip*, vol. 14, no. 16, pp. 2918–2928, 2014, doi: 10.1039/c4lc00464g.

[48] Z. Xu, F. Jiang, Z. Xu, H. Xu, and X. Ruan, "Novel prototyping method for microfluidic devices based on thermoplastic polyurethane microcapillary film," *Microfluid. Nanofluidics*, vol. 20, no. 9, pp. 1–10, 2016, doi: 10.1007/s10404-016-1784-4.

[49] A. Bonyár, H. Sántha, B. Ring, M. Varga, J. G. Kovács, and G. Harsányi, "3D Rapid Prototyping Technology (RPT) as a powerful tool in microfluidic development," *Procedia Eng.*, vol. 5, pp. 291–294, 2010, doi: 10.1016/j.proeng.2010.09.105.

[50] A. Waldbaur, H. Rapp, K. Länge, and B. E. Rapp, "Let there be chip - Towards rapid prototyping of microfluidic devices: One-step manufacturing processes," *Anal. Methods*, vol. 3, no. 12, pp. 2681–2716, 2011, doi: 10.1039/c1ay05253e.

[51] S. A. Rani, B. Pitts, and P. S. Stewart, "Rapid diffusion of fluorescent tracers into Staphylococcus epidermidis biofilms visualized by time lapse microscopy," *Antimicrob. Agents Chemother.*, vol. 49, no. 2, pp. 728–732, 2005, doi: 10.1128/AAC.49.2.728-732.2005.

[52] X. Chen, T. Li, H. Zeng, Z. Hu, and B. Fu, "Numerical and experimental investigation on micromixers with serpentine microchannels," *Int. J. Heat Mass Transf.*, vol. 98, pp. 131–140, 2016, doi: 10.1016/j.ijheatmasstransfer.2016.03.041.

[53] J. N. Kuo and L. R. Jiang, “Design optimization of micromixer with square-wave microchannel on compact disk microfluidic platform,” *Microsyst. Technol.*, vol. 20, no. 1, pp. 91–99, 2014, doi: 10.1007/s00542-013-1769-0.

[54] D. Bošković and S. Loebbecke, “Modelling of the residence time distribution in micromixers,” *Chem. Eng. J.*, vol. 135, no. SUPPL. 1, pp. 138–146, 2008, doi: 10.1016/j.cej.2007.07.058.

[55] S. R. L. Gobert, S. Kuhn, L. Braeken, and L. C. J. Thomassen, “Characterization of Milli- and Microflow Reactors: Mixing Efficiency and Residence Time Distribution,” *Org. Process Res. Dev.*, vol. 21, no. 4, pp. 531–542, 2017, doi: 10.1021/acs.oprd.6b00359.

[56] S. Akar, A. Taheri, R. Bazaz, E. Warkiani, and M. Shaegh, “Twisted architecture for enhancement of passive micromixing in a wide range of Reynolds numbers,” *Chem. Eng. Process. - Process Intensif.*, vol. 160, no. July 2020, p. 108251, 2021, doi: 10.1016/j.cep.2020.108251.

[57] H. Shi *et al.*, “Mixing enhancement via a serpentine micromixer for real-time activation of carboxyl,” *Chem. Eng. J.*, vol. 392, p. 123642, 2020, doi: https://doi.org/10.1016/j.cej.2019.123642.

[58] X. Nguyen, A. Carafa, and C. H. Hornung, “Hydrogenation of vinyl acetate using a continuous flow tubular reactor with catalytic static mixers,” *Chem. Eng. Process. Process Intensif.*, vol. 124, no. December 2017, pp. 215–221, 2018, doi: 10.1016/j.cep.2017.12.007.

[59] T. M. Hamilton, A. A. Dobie-Galuska, and S. M. Wietstock, “The o-Phenylenediamine-

Horseradish Peroxidase System: Enzyme Kinetics in the General Chemistry Laboratory," *J. Chem. Educ.*, vol. 76, no. 5, pp. 642–644, 1999, doi: 10.1021/ed076p642.

[60] W. M. Aumiller, B. W. Davis, E. Hatzakis, and C. D. Keating, "Interactions of macromolecular crowding agents and cosolutes with small-molecule substrates: Effect on horseradish peroxidase activity with two different substrates," *J. Phys. Chem. B,* vol. 118, no. 36, pp. 10624–10632, 2014, doi: 10.1021/jp506594f.

[61] C. Y. Lee, C. L. Chang, Y. N. Wang, and L. M. Fu, "Microfluidic mixing: A review," *Int. J. Mol. Sci.*, vol. 12, no. 5, pp. 3263–3287, 2011, doi: 10.3390/ijms12053263.

Tables

Table 1: Simulated parameters from microchannel structures with equal lengths (110 mm) and equal repeating units at a velocity of 0.003 m/s and diffusion coefficient of $5x10^{-10}$ m^2/s

		ΔP (Pa)	τ (s)	$\bar{t}$ (s)
Equal length	Straight	100.2	36.7	37.0
	Zigzag	147.1	36.7	21.7
	Square	101.0	36.7	37.4
	Wavy	101.3	36.7	36.9
Equal units	Zigzag	88.12	21.7	13.1
	Square	101.2	37.0	37.4
	Wavy	82.90	28.3	29.8

Table 2: Experimental mean residence times for microchannel structures with equal length (320 mm) and equal repeating units at a diffusion coefficient of $5x10^{-10}$ m^2/s with tracer dye

		10 capillaries		Single capillary	
		Tracer (s)	Washout (s)	Tracer (s)	Washout (s)
Equal length	Straight	89.10	84.99	80.57	76.23
	Square	92.68	90.41	83.16	78.99
	Zigzag	88.92	88.89	79.10	77.46
Equal units	Square	92.68	90.41	83.16	78.99
	Zigzag	65.75	63.84	57.88	54.71

Figure captions

Figure 1: (a) Microcapillary Film (MCF) consisting of 10 capillaries with internal diameters of 200 μm. (b) Schematics illustrating dimensions of 3D printed templates for the square geometry with different aspect ratios. (c) The process used for the fabrication of microcapillary structures using the 3D printed template.

Figure 2: (a) Schematics illustrating dimensions corresponding to (b) 3D models used to design template structures. (c) 3D printed templates used to fabricate (d) microcapillary structures. Scale bars represent 10 mm.

Figure 3: (a) 2D planar geometries for 200 μm diameter microchannels with (b) corresponding mesh structures and (c) mesh independence studies. (d) Velocity contour plots for microchannel geometries at 0.05 m/s. (e) Fluid flow shift representation where the position 0 indicates straight flow and -1 and 1 indicates a direction change in the Y axis (a repeating unit is shown by the dashed area).

Figure 4: Breakthrough curves with tracer dye ($5x10^{-10}$ m^2/s) for (a) same length and (b) same unit microstructures for CFD simulations validated with experimental studies at a flow rate of 0.93 μl/s (0.003 m/s). Same length simulations and experiments refer to 110 mm and 320 mm respectively. (c) E-curves for simulations of same length microstructures investigating different velocities and molecular diffusion coefficients. (d) Effect of velocities for square at (i) D_m=$5x10^{-10}$ m^2/s and (ii) D_m=10^{-7} m^2/s. Note that for (a) the straight, square, and wavy are overlapping and have the identical RTD profiles.

Figure 5: (a) Schematic illustrating immobilization of HRP conjugated antibody and enzymatic reaction process converting OPD substrate to DAP product over time. (b) Enzymatic reaction in the MCF converting OPD substrate to DAP product over capillary length and after flow was stopped (MCF removed from inlet solution) with (c) schematic illustrating the role

of diffusion time (t_{diff}) in both flow conditions. (d) (i) Conversion (X) of OPD over reactor length along with (ii) reaction rate over enzyme concentration. (e) Schematic of HRP conjugated antibodies immobilized on microstructure walls. (f) (i) Enzymatic X (2 data sets) and (ii) reaction rates at HRP concentration of 7 μg/ml over axial length for different microstructures where standard deviations were taken from the mean of multiple replicas.

Figures

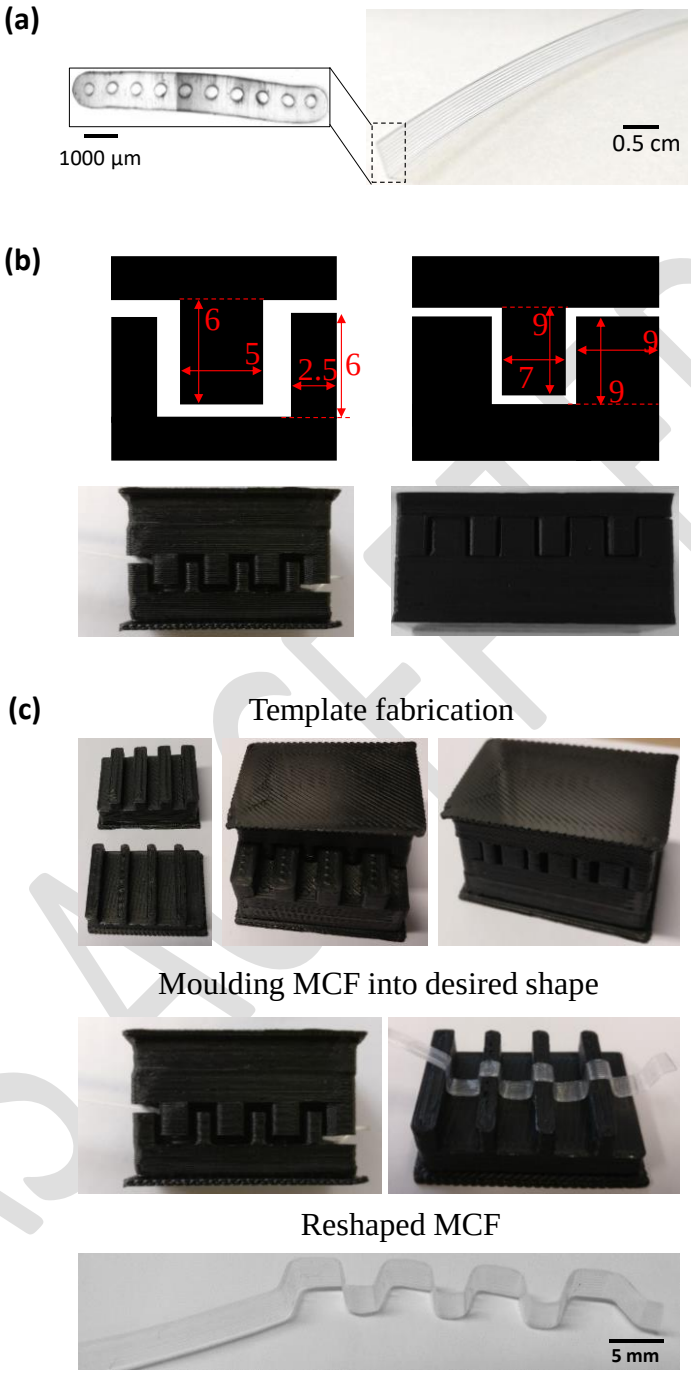

Figure 1

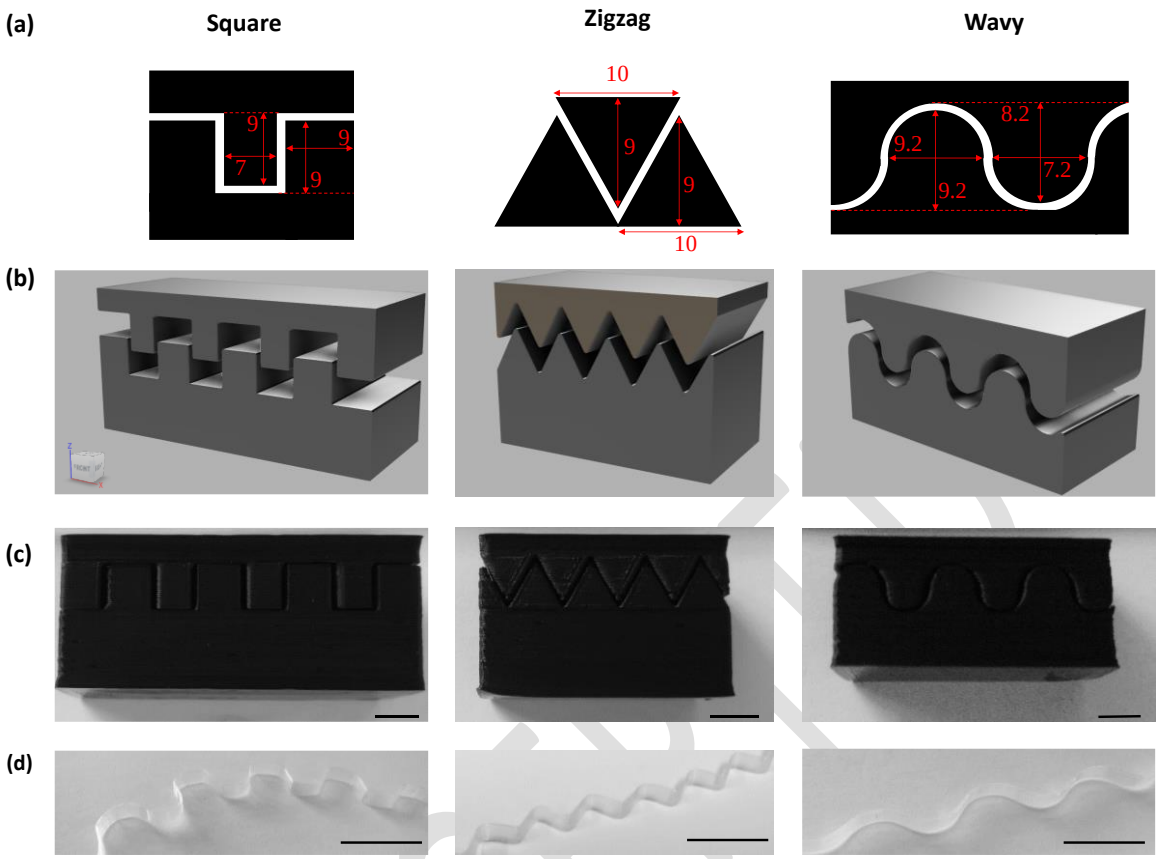

Figure 2

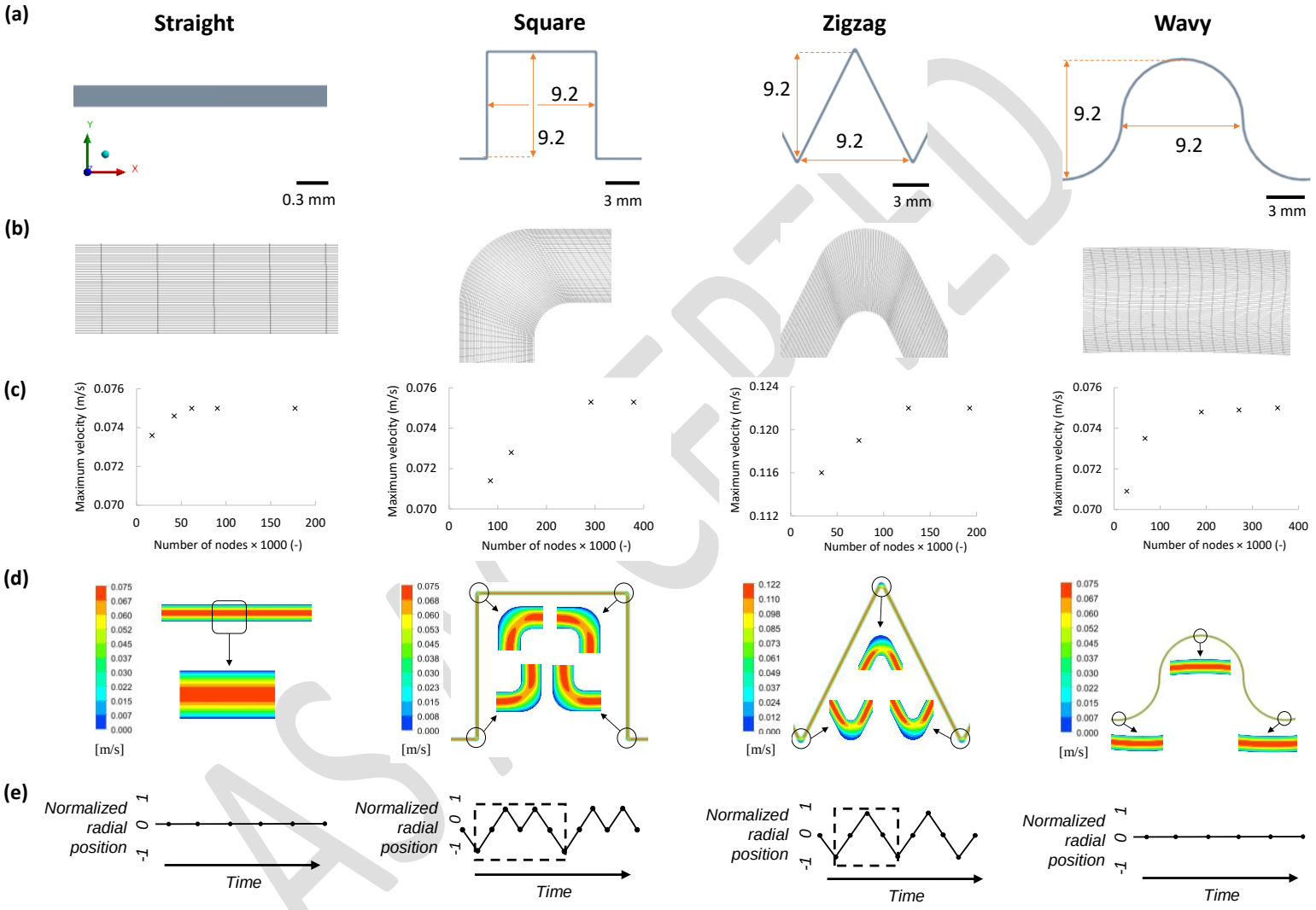

Figure 3

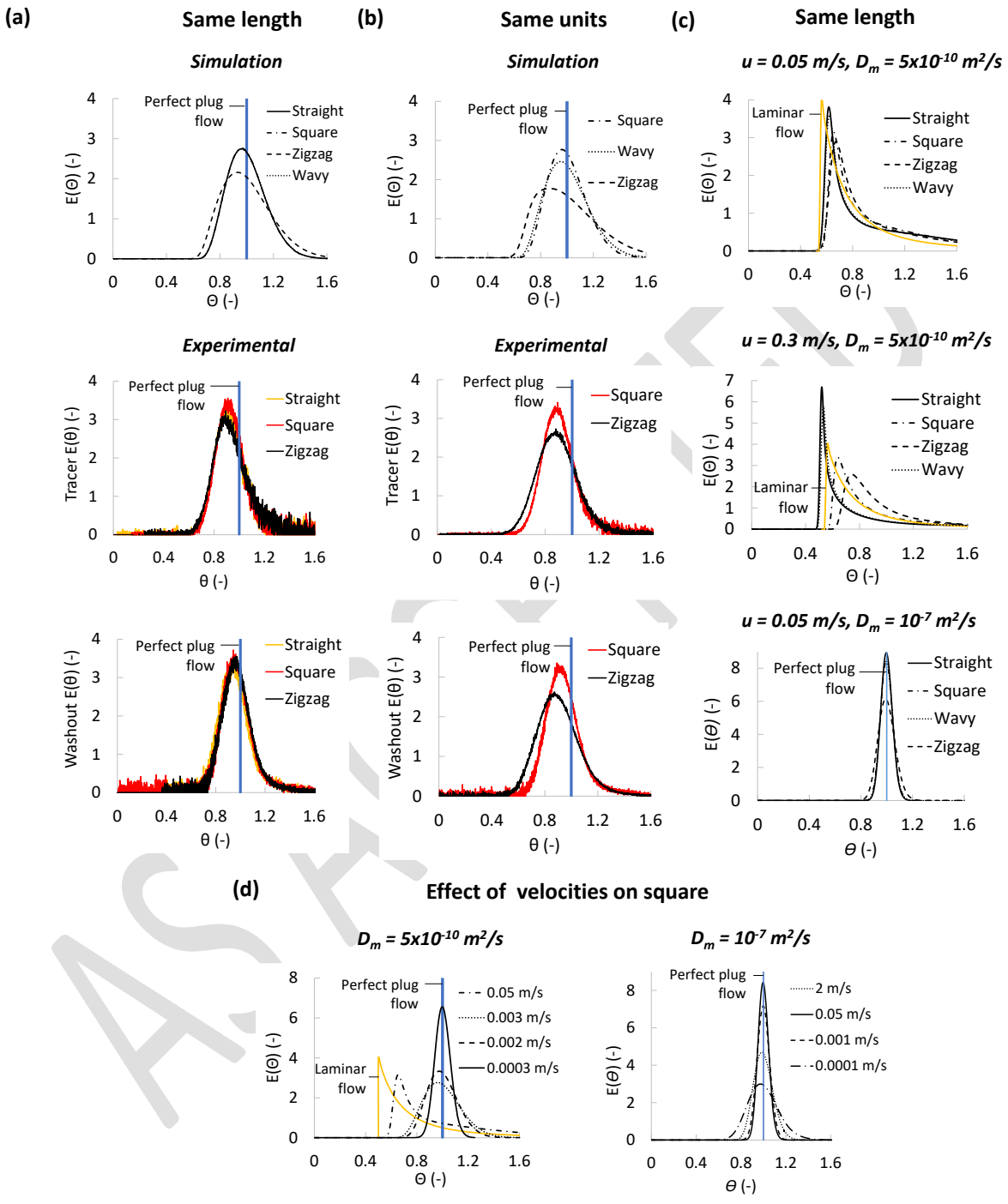
(a)
Same length
Simulation
Perfect plug flow
Straight
Square
Zigzag
Wavy
E(Θ) (-)
Θ (-)
Experimental
Tracer E(θ) (-)
θ (-)
Washout E(θ) (-)
(b)
Same units
Simulation
Perfect plug flow
Square
Wavy
Zigzag
Experimental
Square
Zigzag
(c)
Same length
u = 0.05 m/s, Dm = 5x10-10 m2/s
Laminar flow
Straight
Square
Zigzag
Wavy
u = 0.3 m/s, Dm = 5x10-10 m2/s
u = 0.05 m/s, Dm = 10-7 m2/s
E(Θ) (-)
(d)
Effect of velocities on square
Dm = 5x10-10 m2/s
Dm = 10-7 m2/s
0.05 m/s
0.003 m/s
0.002 m/s
0.0003 m/s
2 m/s
0.05 m/s
0.001 m/s
0.0001 m/s

Figure 4

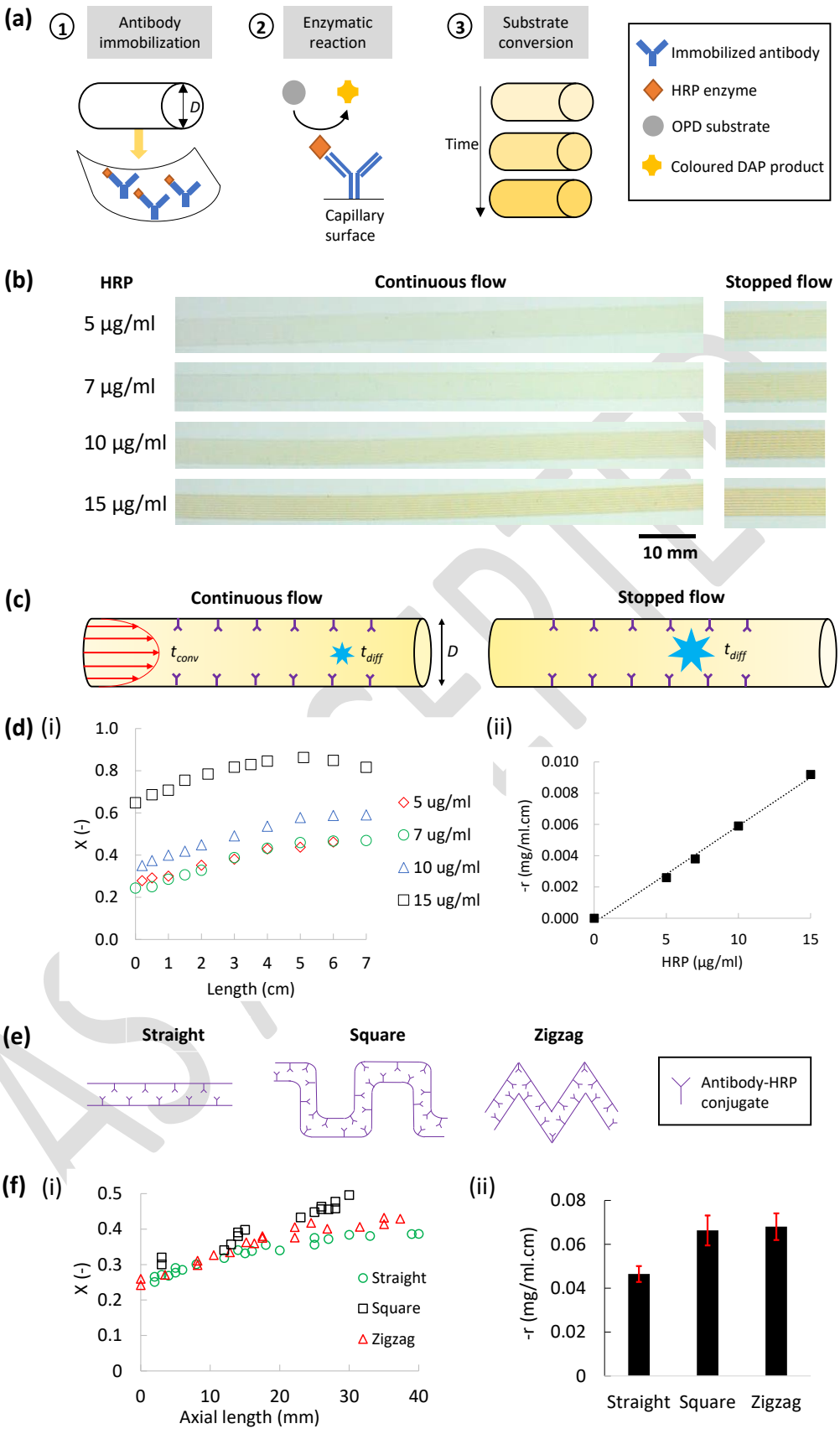
(a)
1 Antibody immobilization
2 Enzymatic reaction
3 Substrate conversion
D
Capillary surface
Time
Immobilized antibody
HRP enzyme
OPD substrate
Coloured DAP product
(b)
HRP
Continuous flow
Stopped flow
5 µg/ml
7 µg/ml
10 µg/ml
15 µg/ml
10 mm
(c)
Continuous flow
Stopped flow
t_{conv}
t_{diff}
D
t_{diff}
(d) (i)
X (-)
Length (cm)
5 ug/ml
7 ug/ml
10 ug/ml
15 ug/ml
(ii)
-r (mg/ml.cm)
HRP (µg/ml)
(e)
Straight
Square
Zigzag
Antibody-HRP conjugate
(f) (i)
X (-)
Axial length (mm)
Straight
Square
Zigzag
(ii)
-r (mg/ml.cm)
Straight
Square
Zigzag

Figure 5